Available online at www.sciencedirect.com

ScienceDirect

Energy Procedia 129 (2017) 50–57

Energy Procedia

www.elsevier.com/locate/procedia

IV International Seminar on ORC Power Systems, ORC2017
13-15 September 2017, Milano, Italy

Deterministic Global Optimization of the Design of a Geothermal Organic Rankine Cycle

Wolfgang R. Huster[a], Dominik Bongartz[a], Alexander Mitsos[a,b,*]

[a]*RWTH Aachen University - Process Systems Engineering (AVT.SVT), Forckenbeckstr. 51, 52074 Aachen, Germany*
[b]*JARA-ENERGY, Templergraben 55, 52056 Aachen, Germany*

Abstract

Herein, a framework for deterministic global optimization of process flowsheets is adapted to the design of an organic Rankine cycle for geothermal power generation. A case study using isobutane as working fluid is considered for the optimal sizing of components and selection of operating conditions at different ambient temperatures. The framework can provide the global optimum in reasonable calculation times within tight tolerances. In contrast, most local solvers applied are found to be inadequate. The CPU times are substantially smaller compared to a state-of-the-art global solver. For the case considered, recuperation can increase net power output but not necessarily economics.

Peer-review under responsibility of the scientific committee of the IV International Seminar on ORC Power Systems.

Keywords: Deterministic Global Optimization; McCormick Relaxations; Organic Rankine Cycle; Isobutane; Geothermal; Techno-economic Optimization;

1. Introduction

The need for more efficient use of energy resources and at the same time growing computational power has made numerical optimization a widely employed tool in process design [1] that has already been applied to the design of organic Rankine cycles (ORC) [2]. However, previous studies have mostly relied on local solvers that only return locally optimal solutions [3]. Since most complex real-world problems are nonconvex [4], they can have multiple local solutions and thus the application of deterministic global optimizers is desirable to guarantee the best attainable solution of the problem. Recently, a new framework has been introduced [5] that makes use of McCormick relaxations [6] and more specifically their extension to the relaxation of algorithms [7] to create convex relaxations of the optimization problem. In contrast to other global solvers [8], it enables the use of the sequential-modular mode which drastically reduces the number of optimization variables seen by the optimizer.

* Alexander Mitsos. Tel.: +49 241 80 94704 ; fax: +49 241 80 92326.
E-mail address: amitsos@alum.mit.edu

1876-6102
Peer-review under responsibility of the scientific committee of the IV International Seminar on ORC Power Systems.
10.1016/j.egypro.2017.09.181

In this contribution, we adapt this solution procedure to globally optimize an ORC for power generation from geothermal brine [9]. While in [9] the off-design behavior of an existing plant was analyzed for varying ambient temperatures, we herein generate optimal design and working conditions for different design scenarios, i.e., attainable cooling water temperatures. These temperatures have an impact on the inlet temperature of the cooling water, that is used to condense the working fluid (WF), and therefore the lower pressure of the ORC. The working fluid, isobutane (R-600a), is also taken from [9], as a promising choice for low evaporating temperatures ($T_{heatsource,in} < 450$ K) [10,11]. Of high importance is the shape of the two-phase region in the temperature-entropy-diagram, as the isentropic expansion in the expander can lead to droplet formation, thus damaging turbine blades. As isobutane is a dry-working fluid (O-type, [9]), this is not the case and superheating is therefore not obligatory. However, as shown in [9], superheating can be of advantage under certain circumstances. Therefore, a superheater in included in the flowsheet, with its sizing considered in this study. The problem is set up as nonlinear program (NLP) with a relatively simple calculation of the physical properties for the WF and a fixed cycle structure and optimized for either maximum net power or minimum levelized cost of electricity. As the purpose of this manuscript is the proof of concept for the optimization framework being applied to the case study, resulting inaccuracies have to be accepted here.

In the following, we first briefly summarize the optimization formulation and solution procedure. Next, the boundary conditions of the case study as well as the models employed are described. Finally, the results for the optimal plant design are discussed along with the required solution times.

2. Global Optimization

Steady-state models for thermal organic Rankine cycles consist of nonlinear equations, resulting from physical relations such as mass and energy balances [3]. Due to these equations, the optimization problems arising when optimizing an ORC typically have nonconvex feasible regions, possibly resulting in multiple local optimal solutions that give substantially suboptimal performance compared to global optima.

Methods for global optimization broadly fall into two categories [12]: Stochastic global optimizers such as, e.g., genetic algorithms, which have been applied in some previous studies on ORC design [13], are only guaranteed to yield a global solution at infinite runtime, and there is no easy way of verifying a given solution is globally optimal. Deterministic global optimizers, on the other hand, terminate in finite time while guaranteeing global optimality to within a specified tolerance. As a range of deterministic global optimizers is available [14,15], the details of the algorithms are not further explained here.

A major characteristic of most available deterministic solvers is that they require the flowsheet optimization problem to be formulated in the so-called *equation-oriented mode*, in which the optimizer has access to all equations and variables. This can lead to high computational times, at least in standard methods, and tight bounds on all variables have to be provided, which can be challenging for bigger problems.

However, as the number of degrees of freedom in process design problems is by far smaller than the total number of model variables of the process, the use of formulations that operate in a reduced space, similar to the so-called *sequential modular mode*, can be of advantage, as shown in [5,7,16]. In this case, the majority of the relations describing the different components of the flowsheet, are rearranged (possibly grouped in modules [17]) so they can be evaluated sequentially, and moved to an external function that the optimizer has no direct access to. These modules act as grey boxes to the optimizer, as it has access only to the given optimization variables.

The solution of this reduced-space formulation is enabled by the automatic propagation of McCormick relaxations [7] through the external functions containing the model equations using the MC++ library [18]. The solver itself is described in detail in [5]. It employs a Branch-and-Bound (B&B) algorithm [19], i.e. it subdivides the search space to derive lower (LBD) and upper (UBD) bounds on the optimal objective value, and the algorithm converges once these become equal to within a given tolerance. For lower bounding, convex relaxations of the external factorable functions provided by MC++ [18] are linearized and the resulting linear program (LP) is solved with the linear programming

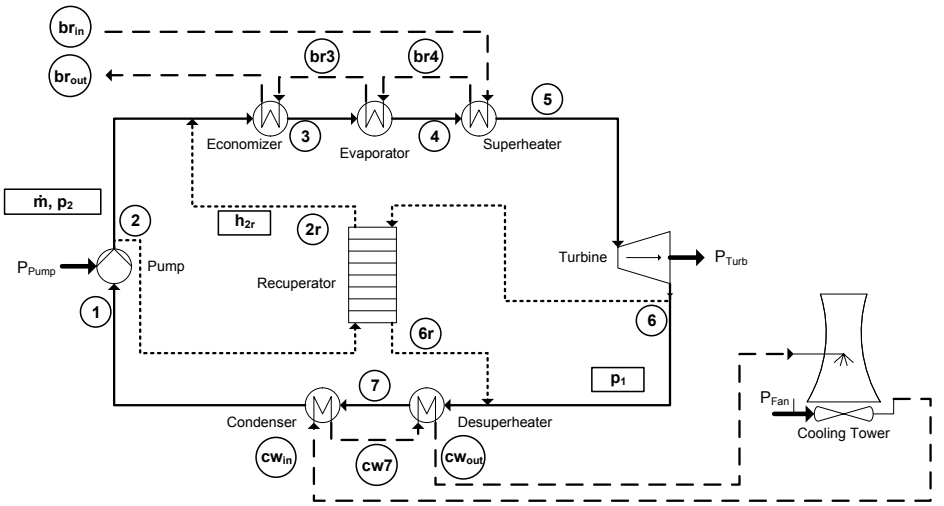

Fig. 1. Overview of the geothermal organic Rankine cycle, including brine and cooling water flows (dashed lines) and the optional recuperator (dotted lines). The states of the fluids are labeled in cycles, while the optimization variables are labeled within rectangles.

solver CPLEX [20]. The upper bounds are found by the local NLP solver SLSQP [21], which is included in the NLopt library v2.4.2 [22]. Note that this setup is a very simple implementation which does not use the latest advances of global optimization as this contribution serves a proof of concept for the optimization framework.

3. Organic Rankine Cycle Model

3.1. Case Study

For the case study of the optimization framework, a geothermal organic Rankine cycle based on the problem of [9] is chosen. As the purpose of this work is the design of the cycle (in contrast to [9]), the structure is simplified to the structure shown in Fig. 1.

Starting at point 1, the WF is pumped to a higher pressure level and afterwards heated to its saturation temperature in the economizer, evaporated and superheated. In our formulation, these three components are modeled separately in order to provide accessibility to the temperatures at each point and the appearing pinch points between the WF and heat source. The conditions of the heat source (geothermal brine) are taken from [9]: starting with an inlet temperature $T_{br,in}$ = 408 K, cooled down to a fixed outlet temperature $T_{br,out}$ = 357 K and a constant heat capacity flow of $\dot{m}_{br} \cdot c_{p,br}$ = 3,627 kW/K. The WF is then expanded in a turbine with a fixed isentropic efficiency. Finally, the WF is cooled to saturation temperature of the low pressure, condensed, and reintroduced to the pump. For the condensation, a cooling water (CW) flow is used with a constant specific heat capacity. After the condenser and desuperheater, the CW is cooled back to its inlet temperature, which is assumed to be a direct function of ambient conditions, in the cooling tower. A total of three different design scenarios are to be analyzed in this work: the CW inlet temperature $T_{cw,in}$ is varied to -5, 0, and 15 °C, representing three different locations of the geothermal field with differing ambient conditions.

The recuperator in Fig. 1, which is often used for dry working fluids [9,23] to make use of the superheated state at the low pressure, is an optional component in this configuration. Using the otherwise nonused heat of the WF after the turbine, a recuperator allows higher WF mass flows for fixed thermodynamic states. As the sizing and therefore the investment costs influences the economic objective function, it does not necessarily improve the system economics. This influence can be seen as a result of the following optimizations. The different scenarios are each optimized once without (basic) and with the use of a recuperator (recup).

All in all the basic model contains 3 degrees of freedom for the working fluid that uniquely define the rest of the process: the high pressure p_{high}, the low pressure p_{low} and the mass flow $\dot{m}_{WF}$. In case the recuperator is used, one additional optimization variable for one exiting stream temperature has to be provided.

All cases are first optimized with regard to the net power P_{net} of the cycle, defined in Eq. (1), which is calculated with the turbine power P_{turb}, the pump power P_{pump}, and the power of the cooling tower fan P_{fan}, which is a function of $\dot{m}_{cw}$ [24].

$$P_{net} = P_{turb} - P_{pump} - P_{fan} \tag{1}$$

Furthermore, all cases are also optimized with regard to the levelized cost of electricity ($LCOE$), which relates the net power to the total capital investment TCI, the equivalent utilization time at rated power T_{eq}, an annuity factor Ψ, a fixed operation cost factor φ and a variable cost factor u_{var}, that is assumed constant, according to Eq. (2) [25].

$$LCOE = \frac{TCI \cdot \Psi \cdot \varphi}{P_{net} \cdot T_{eq}} + u_{var} \tag{2}$$

3.2. Thermodynamic Formulation

In the MC++ framework external third-party thermodynamic libraries or software packages like REFPROP [26] could only be used after adapting the implementation to allow the propagation of relaxations [5]. Therefore, ideal gas and incompressible liquid behavior is assumed with a simple model for heat capacity and enthalpy of vaporization, being sufficiently accurate for this proof of concept. The thermodynamic reference state is chosen to be the saturated liquid state at a reference pressure. Each state of the working fluid is then calculated based on its temperature and pressure. For the calculation of saturation temperatures, the Antoine equation (3) is chosen with parameters from [27] as it is explicit and sufficiently accurate.

$$T_{sat,i} = \frac{B}{A - \log_{10}(p_i)} - C \tag{3}$$

The heat capacity for liquid/vapor states is fitted to data from [26] with a linear dependency of the temperature according to Eq. (4). Liquid enthalpies and entropies can be directly calculated with Eq. (5) + (6), while those in the superheated region are calculated with Eq. (7) + (8). For states in the superheated region, the evaporation enthalpy for the chosen reference state $\Delta h_{evap,p_0}$ is provided [27]. With this formulation, certain inaccuracies are introduced compared to detailed equations of state, but the formulation allows the direct calculation of the temperature for a given enthalpy, as it is for example needed for the calculation of the superheated turbine outlet temperature T_5. In contrast, the fictitious isentropic temperature after the expander $T_{6,s}$ is added, together with the equation $s_5 = s_{6,s}$, as an additional optimization variable, as Eq. (8) can not be explicitly solved for the temperature.

$$c_{p,i} = A_{c_p,i} + B_{c_p,i} \cdot T \tag{4}$$

$$h_{p,liq} = \int_{T_0}^{T} c_{p,liq}\,\mathrm{d}T + \nu_{if} \cdot (p_i - p_0) = A_{c_p,liq} \cdot (T - T_0) + 0.5 \cdot B_{c_p,liq} \cdot \left(T^2 - T_0^2\right) + \nu_{if} \cdot (p_i - p_0) \tag{5}$$

$$s_{p,liq} = \int_{T_0}^{T} \frac{c_{p,liq}}{T}\,\mathrm{d}T = A_{c_p,liq} \cdot \ln\left(\frac{T}{T_0}\right) + B_{c_p,liq} \cdot (T - T_0) \tag{6}$$

$$h_{p,vap} = \Delta h_{evap,p_0} + \int_{T_0}^{T} c_{p,vap}\,\mathrm{d}T = \Delta h_{evap,p_0} + A_{c_p,vap} \cdot (T - T_0) + 0.5 \cdot B_{c_p,vap} \cdot \left(T^2 - T_0^2\right) \tag{7}$$

$$s_{p,vap} = \frac{\Delta h_{evap,p_0}}{T_0} + \int_{T_0}^{T} \frac{c_{p,vap}}{T}\,\mathrm{d}T - \mathrm{R} \cdot ln\left(\frac{p_i}{p_0}\right) = \frac{\Delta h_{evap,p_0}}{T_0} + A_{c_p,liq} \cdot \ln\left(\frac{T}{T_0}\right) + B_{c_p,liq} \cdot (T - T_0) - \mathrm{R} \cdot \ln\left(\frac{p_i}{p_0}\right) \tag{8}$$

3.3. Pinch Assumptions & Heat Exchanger Design

An overview of the streams appearing in heat exchangers within the basic ORC for an exemplary design with minimal superheating is given in Fig. 2. It is assumed that the heat capacity stream of the brine and cooling water does not change with temperature and therefore the curves in the T-$\dot{Q}$ diagram are linear. The minimal temperature difference between brine and working fluid (pinch) appears at the outlet of the economizer. This is usually the case

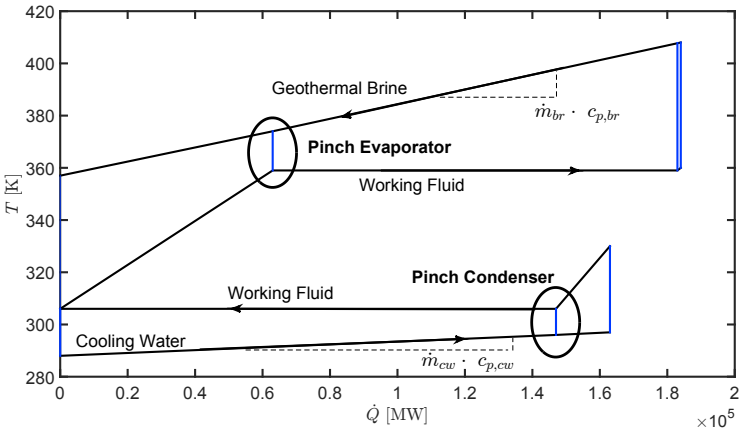

Fig. 2. Pinch points between working fluid and brine/cooling water of evaporator and condenser in a $T - \dot{Q}$ diagram.

for ORCs, as the heat capacity flow of the brine is much higher than of the working fluid in the subcooled region ($\dot{m}_{br} \cdot c_{p,br} \gg \dot{m}_{WF} \cdot c_{p,liq,WF}$). The smallest possible temperature difference at this position is a given parameter of $\Delta T_{pinch,evap} = 15$ K, which is enforced as an inequality constraint. For the condenser, this pinch appears at the condenser inlet, at the kink of the saturated vapor region. It is set to $\Delta T_{pinch,cond} = 10$ K within the model. Through this fixed pinch, the cooling water mass flow is a direct result of the variable lower pressure p_2 of the cycle.

For the design of the heat exchangers, fixed thermal transmittances k_i are introduced, depending on the phase of the contacting fluids. The heat exchanger area A_i is the calculated according to Eq. (9) using Chen's approximation [28] for the mean logarithmic temperature difference (LMTD). Although [29] already provided tight relaxations for the exact LMTD equation, the approximation is used because of the limitations of the other solvers used for comparison.

$$A_i = \frac{\dot{Q}_i}{k_i \cdot \left(\Delta T_{a,i} \cdot \Delta T_{b,i} \cdot \frac{\Delta T_{a,i} + \Delta T_{b,i}}{2} \right)^{\frac{1}{3}}} \tag{9}$$

3.4. Economic Model

For the economic analysis and the calculation of the *LCOE*, the investment costs have to be determined. These costs are summarized by the total costs of all heat exchangers $Inv_{hx,i}$, the pump Inv_{pump}, the turbine Inv_{turb}, and the costs for the cooling tower Inv_{tower}. According to [30], the cost for the power plant of geothermal energy production is only around 42 % of the total installed cost, while the rest includes exploration, drilling etc. In order to not scale these costs with the results of our optimization (since we consider the design of a cycle for a given geothermal source), the fixed value of $Inv_{base} = 22.21$ Mio. US-$, calculated for the base case with an cooling water inlet temperature of 273 K, is added to the investment costs of the power plant for each optimization. The investment costs for the heat exchangers are calculated in dependency of the base purchase cost $C_{p,i}$ (function of A_i) and the pressure factor $F_{p,i}$ (function of the working fluid pressure p_i) according to Eq. (10) [5,31]. Inv_{pump}, Inv_{turb} and Inv_{tower} are depended on their respective power [24].

$$Inv_{hx,i} = 1.18 \cdot \left(1.63 + 1.66 \cdot 2.75 \cdot F_{p,i}\right) \cdot C_{p,i} \tag{10}$$

$$\frac{Inv_{pump}}{\text{US-\$}} = 3540 \cdot \left(\frac{P_{pump}}{\text{kW}}\right)^{0.71} \tag{11}$$

$$\frac{Inv_{turb}}{\text{US-\$}} = 6000 \cdot \left(\frac{P_{turb}}{\text{kW}}\right)^{0.7} + 60 \cdot \left(\frac{P_{turb}}{\text{kW}}\right)^{0.95} \tag{12}$$

$$\frac{Inv_{tower}}{\text{US-\$}} = 1.5 \cdot 10^5 \cdot \left(\frac{P_{fan}}{P_{fan,0}}\right)^{0.6} \tag{13}$$

4. Results

An exemplary projection of a feasible region for the basic ORC is given in Fig. 3. In order to illustrate the feasible region in a two-dimensional plot, the mass flow of the cooling water and thus the lower pressure is fixed. It can be seen that both objective functions improve with higher evaporating pressures. For the illustrated case, the operating conditions for the optimal net power do not coincide with those for the minimal *LCOE*. For reasons of comparison, the full model is formulated in an equation-oriented approach in the optimization framework GAMS [32] to be solved with state-of-the-art solvers. To demonstrate the value of global optimization and the sequential-modular formulation, we also solve the equation-oriented method with different local solvers (CONOPT, IPOPT, SNOPT, KNITRO, MINOS). With the exception of CONOPT, which always finds the global minimum, these fail more often than not. More specifically, the solvers converge to substantially suboptimal solutions (up to 20 %) or even fail to find feasible points. The use of the state-of-the-art global NLP solver BARON [14], in contrast, can validate global optimality of the solutions found by the developed framework. All results could be validated within a given accuracy, guaranteeing the global optimum for a relative gap between LBD and UBD of 10^{-3}, being sufficient with respect to the model accuracy.

The results for the optimization for the three different scenarios of attainable cooling water temperature are given in Tab. 1 for the basic ORC and in Tab. 2 for the recuperated case. For comparison, the CPU times of the MC++ framework and BARON are given. It can be seen that the computational times for the *LCOE* optimization are significantly higher compared to the net power cases because of the increased complexity of the model due to the component sizing and investment cost calculation. This effect can be especially seen for the recuperated case, as the CPU time is increased by a factor 100 for the MC++ framework. The maximal producible net power decreases with increasing ambient and therefore cooling water temperatures, as the condensing pressure increases. The same holds for the minimization of the *LCOE*. But, as shown in Fig. 3, the optimal working conditions do not necessarily coincide and lower *LCOE* can be attained by not producing the maximum power output. Comparing these results with the recuperated case, it can be seen that the recuperator can increase the optimal net power output up to 4 %, depending on the scenario. But, in contrast, for the *LCOE* minimization, the heat exchanger area is always set to its lower bound, indicating that for the given boundary conditions, a recuperator can not improve the economics of the ORC and the results are the same as in the lower half of Tab. 1. The higher CPU times for both solvers result from the increased number of degrees of freedom and equality constraints.

Comparing the *LCOE* results of approximately 40 to 60 US-$/MWh to literature data for geothermal power plants [30,33,34], the attained *LCOE* values are, for binary ORCs of this size, at the lower end of existing plants. For the CPU times of the basic case, the MC++ framework is faster than BARON for every scenario. In the recuperated case in Tab. 2, the new framework is faster for most scenarios. The CPU times show the big potential of the formulation, especially considering our simple implementation compared to the sophisticated technology behind BARON.

Table 1. Results of the net power optimization of the basic ORC case for different design scenarios. The upper subtable displays the results for the maximization of net power, while the lower subtable shows those of the minimization of *LCOE*.

$T_{cw,in}$ [K]	p_1 [bar]	p_2 [bar]	$\dot{m}_{WF}$ [kg/s]	P_{net} [MW]	*LCOE* [US-$/MWh]	CPU time [s]	BARON CPU time [s]
268	2.46	16.8	380	27.3	41.5	1	12
273	2.86	16.5	391	25.3	44.1	2	12
288	4.39	15.4	430	19.0	56.0	1	16
268	2.66	16.6	385	27.1	41.2	2	877
273	3.08	16.3	396	25.1	43.7	2	387
288	4.60	15.2	435	18.8	55.7	3	132

5. Conclusion

The applicability of a developed framework for global optimization with the use of propagating McCormick relaxations is shown using the design of a geothermal organic Rankine cycle plant as case study. The problem can be

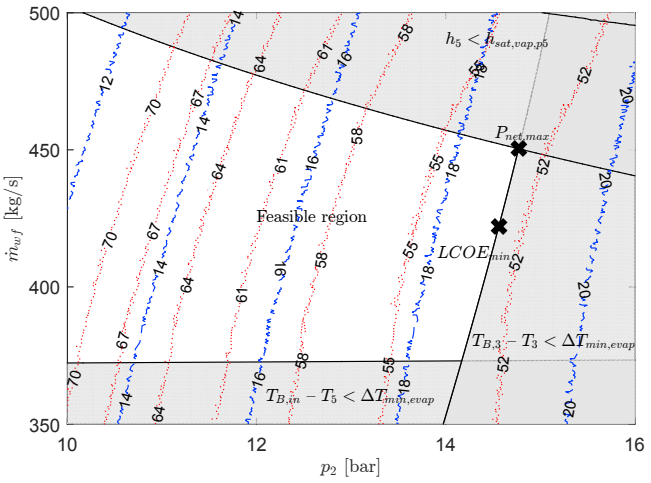

Fig. 3. Resulting feasible region for the basic ORC case with a fixed cooling mass flow. Grey areas display the respective infeasible regions. Dashed lines represent lines of constant net power, dotted lines those of constant *LCOE*.

Table 2. Results of the net power optimization of the recuperated ORC case for different design scenarios. The upper subtable displays the results for the maximization of net power, while the lower subtable shows those of the minimization of *LCOE*

$T_{cw,in}$ [K]	p_1 [bar]	p_2 [bar]	$\dot{m}_{WF}$ [kg/s]	P_{net} [MW]	*LCOE* [US-$/MWh]	CPU time [s]	BARON CPU time [s]
268	2.44	15.9	408	28.4	45.3	12	25
273	2.84	15.7	418	26.1	48.1	7	29
288	4.37	14.8	449	19.1	60.3	12	33
268	2.66	16.6	385	27.1	41.3	1436	3243
273	3.08	16.3	396	25.1	43.8	1817	4765
288	4.60	15.2	435	18.8	55.8	1044	581

solved within reasonable time without the need of bounding of each variable. In contrast, most local solvers using the equation-oriented mode fail to find feasible points or converge to substantially worse solutions.

It is shown that for lower ambient temperatures, more net power can be produced by the cycle, resulting in levelized costs of electricity between 41 and 60 US-$/MWh. While including a recuperator into the cycle leads to higher net powers, the *LCOE* optimization with the use of a recuperator always leads to the minimal recuperator size and same *LCOE* as without recuperator, making this additional component not economical, which is probably caused by the low cost per heat supplied compared to the specific investment costs of an additional heat exchanger.

Ongoing work within the optimization framework includes improvements to the solver to reduce solution times and enable the solution of larger problems. With the ability to handle structural decisions, the ORC could be extended and superstructure optimization be applied. Furthermore, the implementation of more accurate thermodynamic functions, like cubic equations of state, is an important step.

Acknowledgements

The work leading to this contribution was funded by the Federal Ministry for Economic Affairs and Energy (BMWi) according to a resolution passed by the German Federal Parliament. Furthermore, it was partially funded by the German Federal Ministry of Education and Research (BMBF) under grant number 03SFK2A. The responsibility for the content lies with the authors.

References

[1] L. T. Biegler, Nonlinear programming: Concepts, algorithms, and applications to chemical processes, MOS-SIAM series on optimization, Society for Industrial and Applied Mathematics and Mathematical Optimization Society, Philadelphia, 2010.

[2] H. D. Madhawa Hettiarachchi, M. Golubovic, W. M. Worek, Y. Ikegami, Optimum design criteria for an Organic Rankine cycle using low-temperature geothermal heat sources, Energy 32 (9) (2007) 1698–1706.

[3] T. F. Edgar, D. M. Himmelblau, L. S. Lasdon, Optimization of chemical processes, 2nd Edition, McGraw-Hill chemical engineering series, McGraw-Hill, New York, 2001.

[4] L. T. Biegler, I. E. Grossmann, A. W. Westerberg, Systematic methods of chemical process design, Prentice Hall international series in the physical and chemical engineering sciences, Prentice Hall PTR, Upper Saddle River, N.J., 1997.

[5] D. Bongartz, A. Mitsos, Deterministic Global Optimization of Process Flowsheets in a Reduced Space Using McCormick Relaxations. submitted for publication (2017).

[6] G. P. McCormick, Computability of global solutions to factorable nonconvex programs: Part I — Convex underestimating problems, Mathematical Programming 10 (1) (1976) 147–175.

[7] A. Mitsos, B. Chachuat, P. I. Barton, McCormick-Based Relaxations of Algorithms, SIAM Journal on Optimization 20 (2) (2009) 573–601.

[8] M. Tawarmalani, N. V. Sahinidis, A polyhedral branch-and-cut approach to global optimization, Mathematical Programming 103 (2) (2005) 225–249.

[9] H. Ghasemi, M. Paci, A. Tizzanini, A. Mitsos, Modeling and optimization of a binary geothermal power plant, Energy 50 (2013) 412–428.

[10] F. Heberle, D. Brüggemann, Exergy based fluid selection for a geothermal Organic Rankine Cycle for combined heat and power generation, Applied Thermal Engineering 30 (11-12) (2010) 1326–1332.

[11] B. Saleh, G. Koglbauer, M. Wendland, J. Fischer, Working fluids for low-temperature organic Rankine cycles, Energy 32 (7) (2007) 1210–1221.

[12] M. Locatelli, F. Schoen, Global optimization: Theory, algorithms, and applications, MOS-SIAM series on optimization, Mathematical Optimization Society and Society for Industrial and Applied Mathematics, Philadelphia, 2013.

[13] J. Wang, Z. Yan, M. Wang, M. Li, Y. Dai, Multi-objective optimization of an organic Rankine cycle (ORC) for low grade waste heat recovery using evolutionary algorithm, Energy Conversion and Management 71 (2013) 146–158.

[14] M. Tawarmalani, N. V. Sahinidis, Global optimization of mixed-integer nonlinear programs: A theoretical and computational study, Mathematical Programming 99 (3) (2004) 563–591.

[15] R. Misener, C. A. Floudas, ANTIGONE: Algorithms for coNTinuous / Integer Global Optimization of Nonlinear Equations, Journal of Global Optimization 59 (2-3) (2014) 503–526.

[16] M. D. Stuber, J. K. Scott, P. I. Barton, Convex and concave relaxations of implicit functions, Optimization Methods and Software 30 (3) (2014) 424–460.

[17] R. P. Byrne, I. D. L. Bogle, Global Optimization of Modular Process Flowsheets, Industrial & Engineering Chemistry Research 39 (11) (2000) 4296–4301.

[18] B. Chachuat, MC++ (version 2.0): Toolkit for Construction, Manipulation and Bounding of Factorable Functions (2014).
URL http://omega-icl.bitbucket.org/mcpp/

[19] R. Horst, T. Hoang, Global optimization: Deterministic approaches, 3rd Edition, Springer, Berlin and New York, 1996.

[20] International Business Machines Corporation, IBM ILOG CPLEX v12.1 (2009).

[21] D. Kraft, Algorithm 733: TOMP–Fortran modules for optimal control calculations, ACM T. Math. Software 20 (3) (1994) 262–281.

[22] S. G. Johnson, The NLopt nonlinear-optimization package (2017).
URL http://ab-initio.mit.edu/nlopt

[23] H. Ghasemi, E. Sheu, A. Tizzanini, M. Paci, A. Mitsos, Hybrid solar–geothermal power generation: Optimal retrofitting, Applied Energy 131 (2014) 158–170.

[24] M. Lukawski, Design and optimization of standardized organic Rankine cycle power plant for European conditions. MA thesis, RES - The School for Renewable Energy Science (2010).

[25] J. L. Silveira, C. E. Tuna, Thermoeconomic analysis method for optimization of combined heat and power systems. Part I, Progress in Energy and Combustion Science 29 (6) (2003) 479–485.

[26] E. W. Lemmon, Reference Fluid Thermodynamic and Transport Properties Database (REFPROP): Version 9.1 (2013).
URL https://www.nist.gov/srd/refprop

[27] VDI-Wärmeatlas, VDI-Buch, Imprint: Springer Vieweg, Berlin, Heidelberg, 2013.

[28] J. Chen, Comments on improvements on a replacement for the logarithmic mean, Chemical Engineering Science 42 (10) (1987) 2488–2489.

[29] J. Najman, A. Mitsos, Convergence Order of McCormick Relaxations of LMTD function in Heat Exchanger Networks, in: 26th European Symposium on Computer Aided Process Engineering, Vol. 38 of Computer Aided Chemical Engineering, Elsevier, 2016, pp. 1605–1610.

[30] International Renewable Energy Agency, Renewable Power Generation Costs in 2014.
URL http://www.irena.org/menu/index.aspx?mnu=Subcat&PriMenuID=36&CatID=141&SubcatID=494

[31] R. Turton, Analysis, synthesis, and design of chemical processes, 4th Edition, Prentice Hall international series in the physical and chemical engineering sciences, Prentice Hall, Upper Saddle River, NJ, 2012.

[32] GAMS Development Corporation, General Algebraic Modeling System (GAMS) Release 24.6.1 (2016).

[33] G. Mines, J. Nathwani, Estimated power generation costs for EGS, in: 38th Workshop on Geothermal Reservoir Engineering, 2013, pp. 890–895.

[34] V. Stefánsson, Investment cost for geothermal power plants, Geothermics 31 (2) (2002) 263–272.